Frequency stability of optical lattice clocks

2010 New J. Phys. 12 065026

(http://iopscience.iop.org/1367-2630/12/6/065026)

New Journal of Physics
The open-access journal for physics

Frequency stability of optical lattice clocks

Jérôme Lodewyck[1], Philip G Westergaard, Arnaud Lecallier, Luca Lorini and Pierre Lemonde

LNE-SYRTE, Observatoire de Paris, LNE, CNRS, UPMC,
61 avenue de l'Observatoire, 75014 Paris, France
E-mail: jerome.lodewyck@obspm.fr

New Journal of Physics **12** (2010) 065026 (16pp)
Received 11 January 2010
Published 28 June 2010
Online at http://www.njp.org/
doi:10.1088/1367-2630/12/6/065026

Abstract. In this paper, we review several aspects of the frequency stability of optical lattice clocks. We describe a new ultra-stable cavity design with reduced thermal noise and record frequency stability (below 10^{-15}), as well as a non-destructive detection scheme for measuring the clock transition probability. Given the experimental parameters we measured, we simulate different sequence strategies for optimizing the stability. Finally, we report on the development of a second optical lattice clock and simulate several comparison strategies. In particular, we show by a numerical method that a stability as low as $2 \times 10^{-16}\tau^{-1/2}$ can be reached with optical lattice clocks, and we show how to demonstrate this stability with a double clock system.

Contents

1. Introduction 2
2. Stability 3
3. Ultra-stable laser 4
4. Non-destructive detection 6
5. Sequence strategies 7
6. The second Sr optical lattice clock 10
7. Comparing two identical clocks 11
8. Conclusion 13
Acknowledgments 14
References 14

[1] Author to whom any correspondence should be addressed.

1. Introduction

Atomic fountains are currently state-of-the-art atomic clocks in the microwave frequency domain [1–3]. However, hard limits on the stability and accuracy of atomic fountains have now been reached, and there is little hope of significant improvements. Therefore, future developments in atomic clocks are likely to happen in the optical frequency domain, using optical clocks. Indeed, most systematic effects, as well as the dominant and fundamental source of noise in fountains, the quantum projection noise (QPN), do not scale with the clock transition frequency. Thus, the relative accuracy and stability of clocks using an optical transition can, in principle, overcome the microwave standards by several orders of magnitude. However, the Doppler effect scales with the transition frequency, therefore a tight confinement of the atoms during the interrogation period is necessary [4].

Optical lattice clocks, developed first in 2003, consist in locking a narrow-line-width laser on a weakly allowed atomic transition of a large number of atoms trapped in an optical lattice [5–10]. In this configuration, atoms are confined in the Lamb–Dicke regime, in which all motional effects are suppressed [11]. But this mode of operation only works if the frequency difference between the atomic clock levels is unshifted by the trapping potential. This is precisely what happens for a specific wavelength of the optical lattice, the so-called 'magic wavelength' [4, 12].

Optical lattice clocks come as a complementary alternative to optical ion clocks, which offer smaller signal-to-noise ratios (SNRs) in the transition probability measurement due to the limited number of ions that can be trapped together. In practice, ion clocks operate with a single ion. For this reason, whereas the accuracy of the best ion clock is as low as 8.6×10^{-18} [13, 14], its stability is limited to $3 \times 10^{-15}\tau^{-1/2}$ by the QPN given the coherence time of state-of-the-art ultra-stable lasers.

In recent years, huge efforts have been made to improve the accuracy of strontium and ytterbium lattice clocks: by evaluating the hyperpolarizability effects that are not canceled at the magic wavelength [15, 16], by implementing optical pumping schemes [7, 8, 17, 18] and by evaluating the collisional shift [19–22]. With these efforts, the accuracy of optical lattice clocks, at the level of 10^{-16} [6, 8], has already overcome the atomic fountains and is approaching the accuracy of ion clocks. The next step towards increased accuracy involves an accurate determination of the black-body radiation-induced shift. Optical lattice clocks that use other atomic species, such as mercury, are also under development [23].

Comparatively little effort has been made to improve the clock stability, although this is a clear motivation for developing lattice clocks, since the interrogation of a large number of atoms (10^4 to 10^6) has the potential for a large SNR. For instance, a lattice clock with a few 10^4 atoms, a cycle time of 500 ms and an interrogation period of 200 ms, compatible with the current state-of-the-art ultra-stable lasers, has a QPN limit as low as $10^{-17}\tau^{-1/2}$, two orders of magnitude lower than the current frequency stability of ion clocks or the best observed stability for an optical lattice clock ($3 \times 10^{-15}\tau^{-1/2}$ [6]). In this paper, we review several aspects of the frequency stability in optical lattice clocks, as well as experimental improvements we have implemented to reach a high stability level. In section 2, we report on the high-finesse cavity-based laser developed for the strontium clock. The mirrors of this cavity are made of silica, whose nonzero linear thermal expansion coefficient necessitates a high level of thermal insulation. Then, we briefly discuss the non-destructive detection scheme we have developed. This detection scheme helps improve the clock duty cycle, which is a key parameter of the clock

stability. After this, we describe a numerical algorithm used to optimize the clock sequence in order to maximize the stability over the set of possible experimental parameters. In section 6, we report on the status of a second optical lattice clock with strontium atoms under development at LNE-SYRTE. Finally, we discuss several strategies for the comparison of two identical lattice clocks.

2. Stability

The aim of an atomic clock is to cancel the frequency fluctuations of an electro-magnetic (EM) wave (the oscillator, in the microwave domain for atomic fountains or a laser beam for optical clocks) by measuring them with respect to an (absolute) atomic resonance at frequency ν_0. For this purpose, an ensemble of cold atoms are interrogated during a period T by the EM wave. Then, the measurement of the transition probability after the interrogation gives a direct measure of the oscillator noise. To this end, the EM wave frequency is set close to half the resonance maximum where the sensitivity of the transition probability to a given frequency fluctuation of the EM wave is maximal. Quantitatively, for a Ramsey-type interrogation, in which two short $\pi/2$ pulses of duration τ_d are applied, separated by a free evolution period T, the transition probability p as a function of the EM wave frequency ν reads

$$p(\nu) = \frac{1}{2}\left(1 + \cos\left(\frac{2\pi}{2\Delta\nu}(\nu - \nu_0)\right)\right), \tag{1}$$

where $\Delta\nu = 1/2T$ is the resonance full-width at half-maximum. Linearizing equation (1) around the half-maximum of the resonance (at frequency $\nu_{1/2} = \nu_0 - \Delta\nu/2$) yields the relation between a change of the EM wave frequency $\delta\nu = \nu - \nu_{1/2}$ and the departure of the probability δp from $1/2$:

$$\delta p = \pi T \delta\nu. \tag{2}$$

In the following, we will use a general integral formulation of equation (2) valid for any interrogation type:

$$\delta p = \pi \int_{\text{cycle}} g(t)\delta\nu(t)\,\mathrm{d}t, \tag{3}$$

where $\delta\nu(t) = \nu(t) - \nu_{1/2}$ is the instantaneous EM wave frequency excursion from $\nu_{1/2}$, and $g(t)$ the atomic sensitivity function. Outside the interrogation period, $g(t) = 0$. During the free evolution phase of a Ramsey interrogation, $g(t) = 1$ is maximal. For a π/n pulse, $g(t)$ is $2n$th of a sine arch [24, 25]. Of course, for a Ramsey interrogation with $\tau_d \ll T$, equation (3) is identical to equation (2) if we identify $\delta\nu$ with the average of $\delta\nu(t)$ over the interrogation period.

The measurement of δp is used as an error signal to stabilize the EM wave frequency by incrementing the frequency correction ν_{Corr} by $-G\delta p$, where G is the servo-loop gain. In this configuration, $\delta\nu(t)$ not only contains the EM wave (or clock laser for optical clocks) frequency noise itself, but also contains the frequency correction from the servo-loop: $\delta\nu(t) = \delta\nu_{\text{Laser}}(t) + \nu_{\text{Corr}}$. Thus, equation (3) also applies backwards: any additional noise on the transition probability, when fed back to the EM wave through the servo-loop, will induce an additional frequency fluctuation on the locked EM wave.

The first noise source for the transition probability we consider is the noise inherent to the detection system, written as δp_{Det}. According to equation (3), this fluctuation will cause a

frequency fluctuation $\delta p_{\mathrm{Det}}/\pi g_0 T_c$ on the locked EM wave, where g_0 is the average of $g(t)$ over a cycle, and T_c is the cycle time.

A more fundamental noise arises for the measurement of the transition probability. When the atoms are probed at half-maximum, they are prepared in a quantum superposition of the fundamental and excited clock states. The random projections of each atom on either of these states during the detection process introduce noise on the transition probability, written as δp_{QPN}. This noise shows a binomial distribution with a standard deviation $1/2\sqrt{N}$, where N is the number of interrogated atoms. Like the detection noise, this noise is converted into a frequency noise of the locked oscillator by the servo-loop, with standard deviation $1/2\pi g_0 T_c \sqrt{N}$ for a sampling rate of one cycle (equation (3)) . For a given number of atoms, the QPN constitutes a fundamental limitation to the stability of atomic clocks. This level is the actual limitation to the stability of state-of-the-art atomic fountains [2] and could only be overcome by engineering non-classical atomic quantum states, such as spin-squeezed states [26–30]. Still, spin squeezing has never been implemented in an atomic fountain configuration yet, and it has yet to be demonstrated that it does not induce any shift in the clock frequency. However, since the QPN noise level is independent of the clock frequency, its relative effect is much less problematic in optical clocks because the EM wave frequency is several orders of magnitude higher than for atomic fountains in the microwave domain.

The stability is usually characterized by a time-domain analysis called the Allan deviation and written $\sigma_y(\tau)$ [31]. It can easily be computed in a single pass from a finite data set x_i sampled at period t_s with the formula

$$\sigma_y^2(kt_s) = \tfrac{1}{2}\langle (y_{n+1} - y_n)^2 \rangle_n, \tag{4}$$

where y_n is the average of x_i from $i = nk$ to $i = (n+1)k - 1$. For a white noise with a constant power spectral density $S(f) = h_0$, the Allan deviation reads $\sigma_y(\tau) = \sqrt{h_0/2\tau}$, illustrating the time averaging of the white noise. For a flicker noise with a power spectral density $S(f) = h_{-1}/f$, the Allan deviation is constant: $\sigma_y(\tau) = 2\ln(2)h_{-1}$.

3. Ultra-stable laser

One of the key components of an optical clock is the master oscillator, namely a narrow-linewidth laser. In all the optical clock setups built so far, this narrow laser is produced by locking the frequency of a laser beam on a high-finesse optical cavity. This scheme has already enabled lasers with line widths below 1 Hz [32–34].

The technical challenge that has to be met when building such cavities is the control of external perturbations that influence the cavity length. If one wants to stabilize a laser below 1 Hz, i.e. below 10^{-15} in fractional units for optical clocks, the relative fluctuations of the cavity length itself have to be lower than 10^{-15}. This involves isolating the cavity from vibrations as well as thermal fluctuations. To this aim, cavities are usually made with ultra-low expansion (ULE) glass operated close to the inversion point where the linear component of the expansion coefficient is canceled, and put under vacuum in a damped acoustic environment on an anti-vibration table.

The main residual limitation to such a cavity stabilization scheme is the thermal noise of the mirror substrate [35]. This thermal noise level is determined by the material properties and is the current limitation in state-of-the-art ultra-stable lasers. To reduce this effect as much as

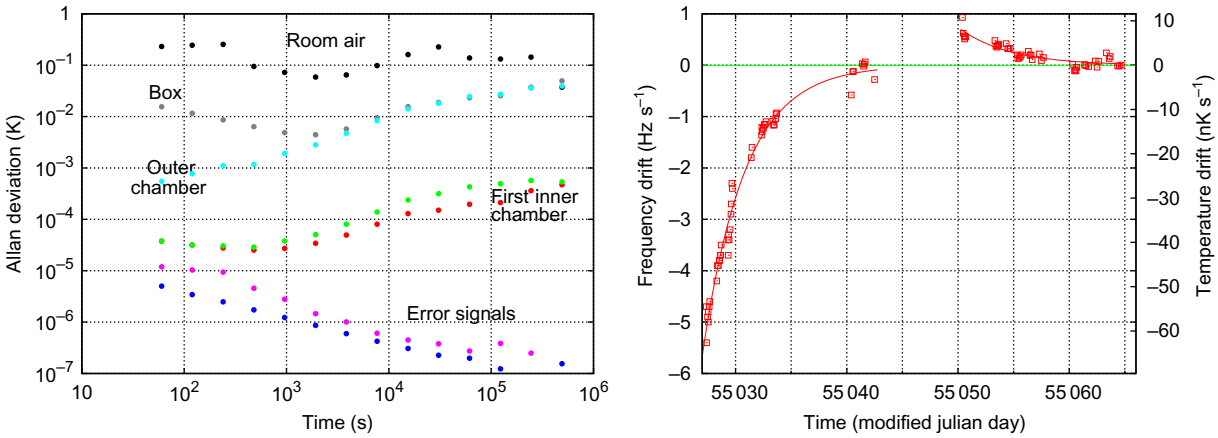

Figure 1. Left: Allan deviation of the temperature of the room air (black), the acoustic box air (grey), the outer vacuum chamber (light blue), the temperature-controlled inner vacuum chamber (two thermistance probes are placed on each side of the chamber: green and red points), and the two servo-loop error signals (purple and dark blue). The temperature of the inner vacuum system is controlled down to a few 0.1 mK. Right: frequency drift of the cavity compared to an old independent all-ULE cavity at 698 nm. It enables us to infer the actual temperature fluctuations of the cavity itself (shown on the right axis, assuming a thermal expansion of $2 \times 10^{-7}\,\mathrm{K}^{-1}$). The graph shows the settling of the initial temperature control as well as the response to a temperature impulse. Both exhibit a time constant of 4.5 days. Even though we are operating at 298 K, far away from the inversion point of the temperature sensitivity (253 K), the stationary drift remains well below $1\,\mathrm{Hz\,s^{-1}}$. A comparison with the microwave cryogenic oscillator at LNE-SYRTE gave an absolute value of $163\,\mathrm{mHz\,s^{-1}}$ for this drift, and it is still dropping.

possible, the cavities we have designed are made with silica mirrors positioned on a ULE spacer. Fused silica exhibits a higher mechanical Q than ULE, which explains why the thermal noise is reduced. Finite element simulations on a horizontal design have been performed to reduce the sensitivity to vibrations [36]. In return for its good thermal noise properties, silica has a greater thermal expansion coefficient than ULE. For this reason, great care has to be taken to shield the cavity from thermal fluctuations in the environment[2]. For this purpose, we designed a double vacuum enclosure. The outer vacuum system is devoted to the temperature control of the inner vacuum system: Peltier elements are glued on each side of the inner chamber and connected to the outer vacuum chamber by a conducting copper braid, itself temperature controlled by Peltier elements. The set points of the temperature controls are 298 K, and they are fine-tuned to cancel any thermal flux inside the chamber. The stability of the temperature stabilization is shown in figure 1. The pressure in the outer vacuum chamber is about 10^{-5} mbar, limited by the outgazing of the Peltier elements and the glue. In the inner vacuum system, three gold-coated thermal shields protect the cavity. The pressure in this inner chamber is 5×10^{-8} mbar.

[2] Another strategy would be to compensate for the high expansion coefficient of silica with a special cavity design [37].

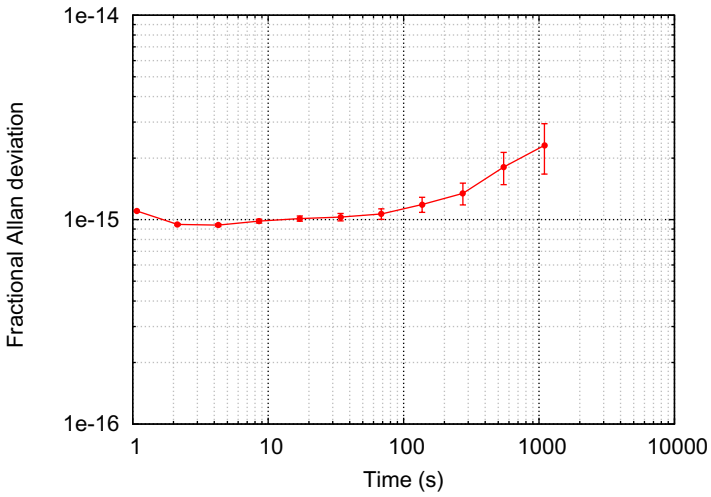

Figure 2. Frequency stability of the de-drifted beat of the strontium cavity against the mercury cavity (1062 nm) measured through a Ti:sapphire femtosecond laser [38]. It shows a frequency noise level around 9×10^{-16}, giving expectedly 6×10^{-16} for at least one of the ultra-stable lasers. This result is close to the expected theoretical thermal flicker noise level of the mirror substrate (around 5×10^{-16}). Some work still remains to fully analyse the fluctuations shown on the plot.

Our clock laser, operating at 698 nm, has been compared with a similar (but vertical) ULE cavity at 1062 nm through a femtosecond laser comb and features a stability shown in figure 2.

4. Non-destructive detection

By nature, a lattice clock works in a cyclic way. A clock cycle, whose duration is of the order of one second, consists of a loading part during which the atoms are cooled and trapped in the lattice, a state preparation part that involves side-band cooling and optical pumping. Then comes the actual interrogation of the atoms by the ultra-stable laser with a Rabi or Ramsey probing. Finally, a measurement of the transition probability gives the error signal used to lock the clock laser. The dead time of a clock cycle is the cycle time minus the interrogation time. During this dead time, the laser frequency fluctuations are not measured (as seen in equation (3) since $g(t) = 0$ during the dead time) and hence cannot be corrected. The dead time degrades the long-term stability of the clock through a sampling effect called the Dick effect [25, 39, 40]. It is noteworthy that this sampling effect involves the laser frequency noise at multiple frequencies of the clock cycle. Then, when considering only the Dick effect, the long-term stability of the clock is limited by the short-term behavior of the laser. A decrease in the impact of the Dick effect can therefore be achieved by reducing the laser noise, which was the aim of the previous section, or by increasing the clock duty cycle d, defined as the ratio between the interrogation time and the total cycle time.

In the operation of most lattice clocks, the measurement of the transition probability implies a complete loss of the atoms. This leads to a large part of the dead time being spent in loading atoms in the optical lattice at the beginning of each cycle. To

avoid losing atoms and hence increasing the duty cycle, we have developed a non-destructive detection scheme for optical lattice clocks. This scheme is fully described in [41]. In this section, we briefly summarize the results and advantages of this detection scheme.

The non-destructive detection relies on the measurement of the phase shift induced by the dispersive properties of an atomic medium on light whose frequency is close to an atomic resonance. This method has already been used with cold atoms to squeeze the total spin of the atomic ensemble [26–29]. To measure this phase shift, we built a Mach–Zender interferometer at 461 nm, composed of a strong reference arm and a low-power (about 10 nW) probe arm that propagates along the optical lattice. Then, a homodyne detector collects the light at the two output arms of the interferometer. To be immune from technical phase fluctuations between the two arms of the interferometer, we phase modulate the probe with an electro-optics modulator. Demodulating the RF output of the detector then gives the differential phase shift between two modulation side bands, which is proportional to the number of atoms in the fundamental clock state. The noise level we achieved with this detection is fundamentally limited by the phase component of the shot noise of the feeble probe. This noise can only be decreased by increasing the probe power, which would result in photon scattering, thence atomic loss. Therefore, the only way to improve the SNR of the detection is to increase the optical density of the atomic population so that the induced phase shift is higher. Thus, only a few parameters can be tuned: firstly, a transition with a larger wavelength could be chosen, but no other convenient cycling transition exists for strontium. Secondly, an increased number of atoms would yield a larger SNR. However, it would also require a longer loading time, hence degrading the stability through the Dick effect. Furthermore, a significantly larger number of atoms would degrade the clock accuracy because of collisional shifts [19–21]. The last possibility would be to use a cavity to enhance the interaction length between the probe and the atoms [29].

The transition probability is measured with a sequence of three phase measurements (a reference pulse, and two pulses separated by a repumping beam). The noise on this measurement has a standard deviation of $200/N$ per cycle, where N is the number of atoms. While it is already competitive with the standard fluorescence detection, there is still little room for improvement with respect to the shot noise limit explained in the previous paragraph.

We characterized the non-destructive aspect of the detection by measuring the fraction of atoms that stayed in the trap after the interrogation sequence. For deep lattices (about 400 recoil energies at 461 nm), more than 95% of the atoms remain in the trap after detection of the transition probability.

5. Sequence strategies

In [42], we explored several sequence strategies that can benefit from an improved clock laser associated with a non-destructive detection scheme. In particular, a trade-off between a long loading time that increases the number of atoms and a short loading time that increases the duty cycle was found. This numerical approach consists of evaluating the expected frequency stability $\sigma_y(\tau)$ of the clock by considering the variances of the different noises that impact the transition probability (δp_{Det} and δp_{QPN}), as well as the impact of $\delta \nu_{\mathrm{Laser}}$ by a Fourier series analysis of the Dick effect. From this study, we could estimate the stability that can be

expected with our experimental parameters. In particular, it was shown that a stability as low as $2 \times 10^{-16}\tau^{-1/2}$ could be achieved. However, these simulations suffered from several limitations:

- The type of sequences explored were limited to periodic sequences in which an atom loading phase is triggered at the beginning of *each* sequence. However, the non-destructive aspect of our detection enables us to adopt non-periodic schemes in which we load a large number of atoms at a time, at the expense of a long loading time, but then perform several clock interrogation cycles with the same atomic ensemble. With this kind of sequence, the average loading time could be reduced by eliminating dead times in the loading process. Furthermore, it would be particularly adapted to loading techniques in which large numbers of atoms can be accumulated after a multi-step sequence (see, for instance, [43, 44]). However, the linear model used in [42] becomes quite intractable in this configuration, and other numerical techniques have to be employed.
- In the short term, i.e. for timescales smaller than or comparable to the clock cycle, the stability of the locked oscillator is limited by the stability of the free oscillator (namely the ultra-stable laser). Only after several clock cycles can the atomic lock bring the stability down to the stability expected from the atomic response. The results obtained in [42] were only valid for large timescales for which this regime is attained. This is justified by the relatively short clock cycle duration associated with the non-destructive detection. However, for large duty cycles, the expected level of the Dick effect can be quite low and a significant integration time might be necessary to reach this level. Here, we show quantitatively when this regime is reached.
- The noise of the ultra-stable laser we used in [42] was chosen to be the theoretical thermal flicker noise level for silica mirror substrates. Here, we also study the effect of other potential noise sources, such as white noise.

To take into account these aspects, we describe in this paper an alternative optimization method that consists in the step-by-step numerical simulation of the full-clock operation. Each clock cycle with duration T_c is divided into 100 time steps. At each step, the laser noise $\delta\nu_{\text{Laser}}$ is generated by a congruential long-period pseudo-random generator and is used to compute integral (3). At the end of the cycle, the detection noise δp_{Det} with standard deviation $200/N$ is generated by a Gaussian white noise random generator and the QPN is generated by a binomial random generator. Finally, the frequency correction ν_{Corr} to apply to the laser is incremented by $-\delta p_{\text{Tot}} G$, where

$$\delta p_{\text{Tot}} = \pi \int_{\text{cycle}} g(t)\,(\delta\nu_{\text{Laser}}(t) + \nu_{\text{Corr}})\,\mathrm{d}t + \delta p_{\text{Det}} + \delta p_{\text{QPN}}. \tag{5}$$

The lock gain G is adjusted to minimize the variance of the corrected frequency using the golden section algorithm. This methodology directly implements the servo-loop algorithm analytically studied in [40]. With it, we can easily simulate sequences with irregular patterns, or with a varying number of atoms from cycle to cycle.

This algorithm has two different frequency outputs. The first one (hereafter called output 1) is the average of the laser frequency $\delta\nu(t) = \delta\nu_{\text{Laser}}(t) + \nu_{\text{Corr}}$ over one clock cycle. Because this output does not include the short-term fluctuations of the laser frequency inside the clock cycle, it is not representative of the actual frequency noise of the locked oscillator at timescales in the order of or faster than the clock cycle time. Consequently, it does not answer the second point we raised above. However, it clearly indicates the asymptotic frequency stability behavior for

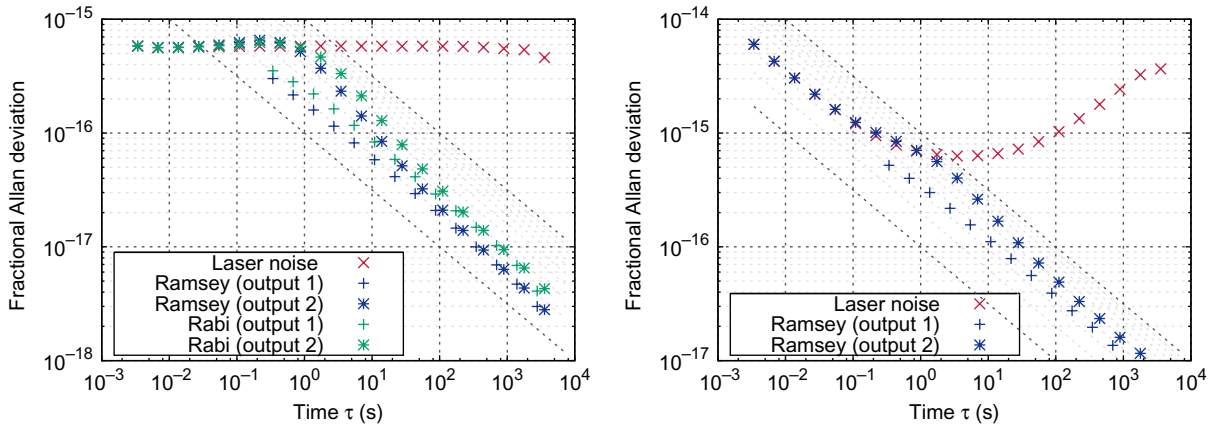

Figure 3. Simulated Allan deviation for an optimal sequence as found in [42] (cycle time $T_c = 340\,\text{ms}$, interrogation time $T = 200\,\text{ms}$, duty cycle $d = 0.59$, number of atoms $N = 4000$). Left: '$\times$' points indicate the laser noise modeled by a flicker noise of spectral rms power density $S(f) = h_{-1}/f$ with $h_{-1} = 0.04\,\text{Hz}^2$, with a corresponding constant Allan deviation of 5.7×10^{-16}. '+' points indicate the Allan deviation of the average laser frequency noise over one cycle, with the lock correction applied (output 1). It corresponds to the asymptotic white noise behavior $\sigma_y(\tau) = 2 \times 10^{-16}\tau^{-1/2}$, as found in [42]. '$*$' points show the Allan deviation of the locked oscillator compared with an independent (noiseless) oscillator (output 2). For timescales shorter than the clock cycle, the frequency noise is limited by the laser. Then, the noise rapidly decreases until it reaches the $1/\sqrt{\tau}$ averaging, around 100 s. These curves are shown for Rabi and Ramsey interrogation schemes. They clearly show the advantage of using a Ramsey interrogation, even for the chosen limited duty cycle. In the following figures, we therefore only consider Ramsey interrogations. Right: the same as the left graph, with the exception that a white frequency noise component with a power spectral density $S(f) = h_0$ with $h_0 = 0.045\,\text{Hz}^2\,\text{Hz}^{-1}$ and a random walk frequency noise component with a power spectral density $S(f) = h_{-2}/f^2$ with $h_{-2} = 4.3 \times 10^{-4}\,\text{Hz}^3$ are added to the flicker frequency noise component of the laser to better model a realistic noise. Because it only concerns large timescales, the random walk noise does not impact the locked laser frequency stability through the Dick effect. However, we see that the white frequency noise component drastically limits the long-term stability of the clock at a level comparable with the white noise level itself (up to 3.5×10^{-16} from $1.9 \times 10^{-16}\tau^{-1/2}$ in the left figure).

timescales much larger than the clock cycle, and then can be directly compared to the analytical formula given in [25, 39] and used in [42]. The second output (output 2) includes the corrected frequency fluctuations for each time step used to compute integral (3). It is the actual frequency noise of the locked oscillator compared to an independent (noiseless) oscillator. The stability curves presented in this paper show both outputs.

Using this algorithm, we simulated the Allan deviation of the optimal sequence found in [42] (figure 3). As expected, the algorithm gives the same asymptotic stability as found in [42], as well as the same individual contribution for each noise component (Dick effect,

detection noise and QPN). It also shows that the asymptotic stability is reached in about 100 s. Figure 3 also shows the frequency stability of the locked oscillator in the presence of white and random walk frequency noise, in order to better model the laser frequency noise observed in figure 2. We can see that, the white noise level of figure 2 is incompatible with the frequency stability solely expected from the flicker frequency noise of the ultra-stable laser. However, this white noise level most probably comes from the frequency transmission system rather than the laser itself, so that it can hopefully be dwarfed.

We now simulate irregular atom loading patterns. Usually, loading the atoms in the optical lattice is not a linear process with time. This is particularly true when several successive trapping and cooling stages are necessary to achieve the dipole trapping (for instance, in schemes that necessitate second stage cooling using a red magneto-optical trap (MOT) [45] or magnetic trapping [43, 44]). In our experiment, this effect is somewhat limited because of the drain technique we use to directly load the atoms from the blue MOT to the optical lattice [46]. Indeed, with this scheme, after the 12 ms needed to load the MOT, the atom loading process is effectively linear. We may still wonder if an irregular sequence pattern could be favorable, in which a large number of atoms could be loaded in a long time relative to the clock cycle and then several successive clock interrogations are performed without reloading the lattice in between. This kind of sequence would be particularly adapted to multi-stage atom loading schemes. We used our algorithm to simulate such sequences. We start with a large number of atoms N and then, at the end of each cycle, the number of atoms is decreased by the losses due to the detection (5%) and the limited lifetime of the trap (set to 4 s). When the number of atoms reaches a chosen low level N_{min}, a few dead cycles n_{d} are spent to reload the optical lattice up to the original number of atoms N. Typically, 700 ms are required to fully refill the optical lattice, which gives $n_{\mathrm{d}} \simeq 3$. Figure 4 shows the asymptotic clock frequency stability obtained with such sequences. We can see that, even with the optimistic values we chose for N and n_{d}, these sequences hardly match the regular pattern, even though the effective duty cycle is higher than the duty cycle of the regular pattern and the average detection noise and QPN are smaller because the number of atoms is always higher. This could be attributed to the fact that irregular patterns introduce low frequencies in the sampling effect of the laser noise.

6. The second Sr optical lattice clock

The strontium optical lattice clock is currently the only lattice clock in operation at LNE-SYRTE, and optical-to-optical comparison is required to demonstrate stabilities as low as stated in the previous section. For this purpose, we are building a second optical lattice clock with strontium atoms, based on the same design as the first lattice clock. A few elements are nonetheless different.

First of all, the atomic beam is deflected by a laser beam before the Zeeman slower (figure 5). This defection has several effects. Firstly, it bends the atomic beam so that there is no direct view of the strontium oven from the trapping area. Thus, this reduces the black-body radiation seen by the trapped atoms, as well as collisions with the atomic beam. In addition, the deflector acts as a collimator, which increases the number of trapped atoms by a factor of 4 with an optical power of 30 mW (figure 5).

Secondly, the laser source for the dipole trap is made of semiconductor sources instead of a Ti:sapphire laser as employed in the first experiment. We used an extended cavity laser diode amplified by a tapered amplifier, giving a total power of 1.4 W at 813 nm. Of this power,

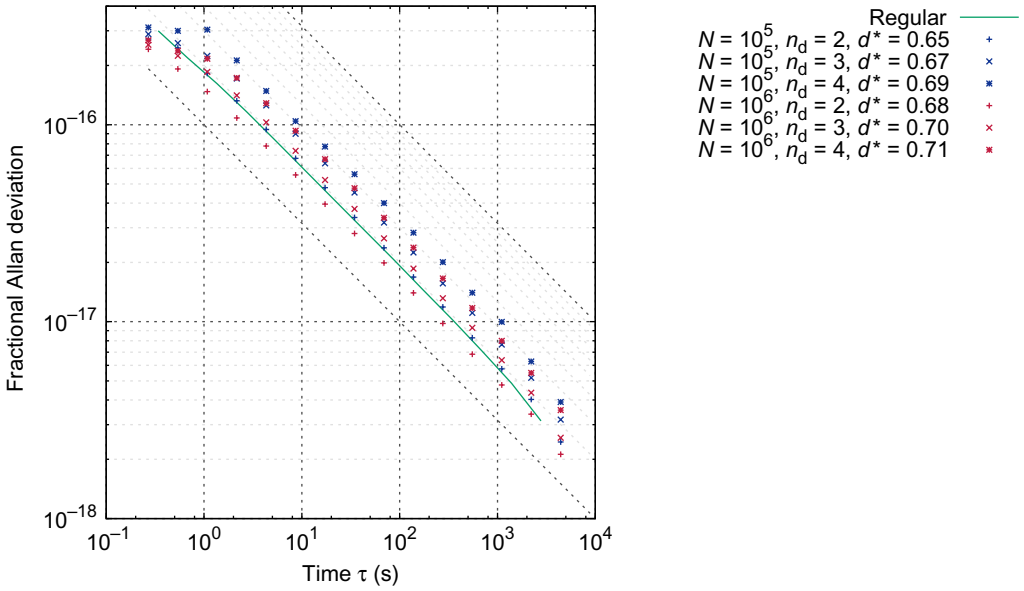

Figure 4. Simulated Allan deviation for irregular sequence patterns. Circles (•) show the asymptotic frequency stability (output 1) for the same regular sequence as for figure 3 (left) for which $d = 0.59$. The other curves show the asymptotic stabilities for irregular sequences with $T = 0.2$ s, $T_c = 0.27$ s (the 70 ms that were required to load the lattice in the regular sequence are removed) and various values for N and n_d, and $N_{min} = 4000$. For a time $t \gg T_c$, we define the effective duty cycle d^* as the ratio between the total time spent interrogating the atoms and t.

500 mW is injected into an optical cavity around the vacuum chamber that forms the optical lattice with an average power of 8.5 W. However, the laser diode frequency noise is converted into amplitude noise by the optical cavity, resulting in a spurious heating of the atoms and hence a prohibitively low lifetime of the atoms in the optical lattice. To reduce this effect, an independent confocal Fabry–Pérot cavity with a line width of 10 MHz is used to lock the master extended cavity laser diode using a Pound–Drever–Hall lock. With this stabilization, we could trap 2×10^3 atoms in the optical lattice and perform a first Lamb–Dicke spectroscopy of the clock transition. Work aimed to optimize the number of trapped atoms is currently underway.

7. Comparing two identical clocks

Comparing two clocks operating at the same frequency is straightforwardly done by measuring the frequency fluctuations of the beat between the two locked oscillators (figure 6(a)). If the two clocks feature identical frequency stabilities, the stability of the beat amounts to $\sqrt{2}$ times the absolute frequency stability of a single clock.

However, for our two strontium clocks, we only have one ultra-stable laser at our disposal. Thus, the two clocks are not strictly independent, and the beat between the two locked oscillators is actually the difference between the two frequency correction signals (figure 6(b)). Figure 7 shows a simulation of this signal for different sequence strategies: a synchronous operation for which the two interrogation periods strictly overlap, an anti-synchronous operation for which

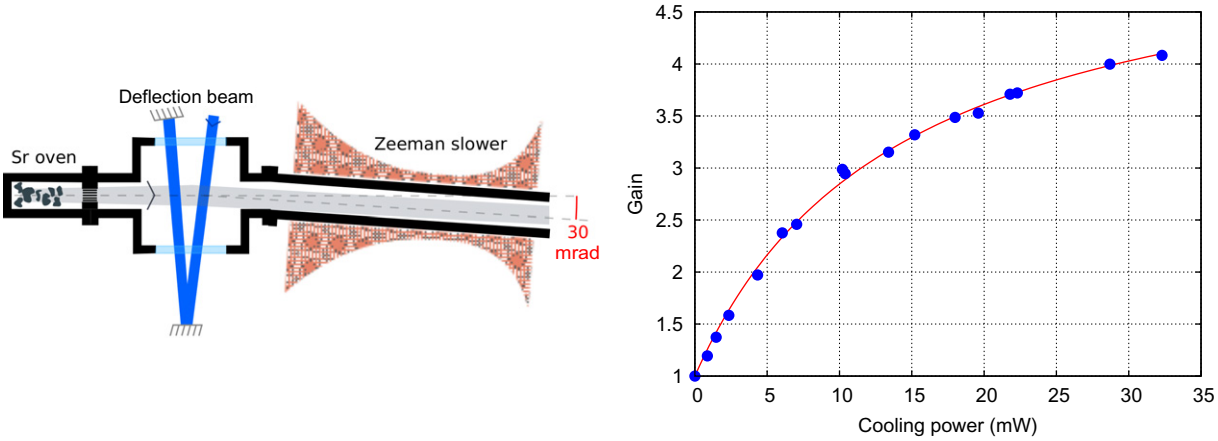

Figure 5. Laser deflector on the horizontal plane using a V-shaped retroreflected laser configuration. The laser beam coming out of the deflection path is then used to collimate the atomic beam in the vertical direction. The laser power is 20 mW, with a 3 mm $1/e^2$ radius. The angle between the two deflecting beams is 100 mrad and the atomic deflection is 30 mrad. The collimation of the atomic beam increases the number of trapped atoms in the MOT by a factor of 4 when the transitions are saturated. This gain is shown in the plot on the right as a function of the power in a linear configuration with collimation but without deflection. The experimental points are fitted with a saturation curve. The same number of atoms can then be achieved in a deflection configuration.

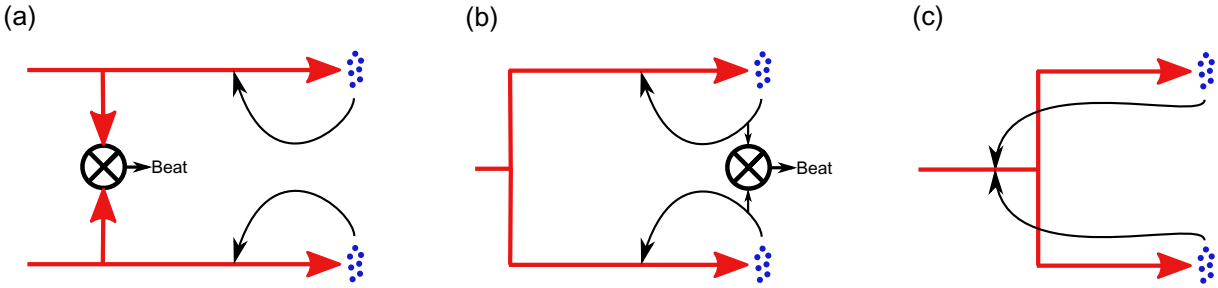

Figure 6. Clock comparison schemes considered in section 7. Red arrows symbolize the clock laser beam, and black arrows represent the frequency corrections deduced from the measurement of the atomic transition probabilities.

the two interrogation periods are strictly disconnected, and a random operation for which the relative positions of the interrogation windows is uniformly random. The latter operation is equivalent to two clocks having slightly different clock cycle times T_c.

In the synchronous sequence, the two clocks sample the laser noise at the same time. Therefore, a frequency noise level below the level of the Dick effect can be reached. We find that the stability of the difference of the frequency corrections of the two clocks with randomly triggered interrogation windows is at the same level as the asymptotic behavior of the actual beat between two independent clocks (output 1, as defined in section 5). We emphasize that

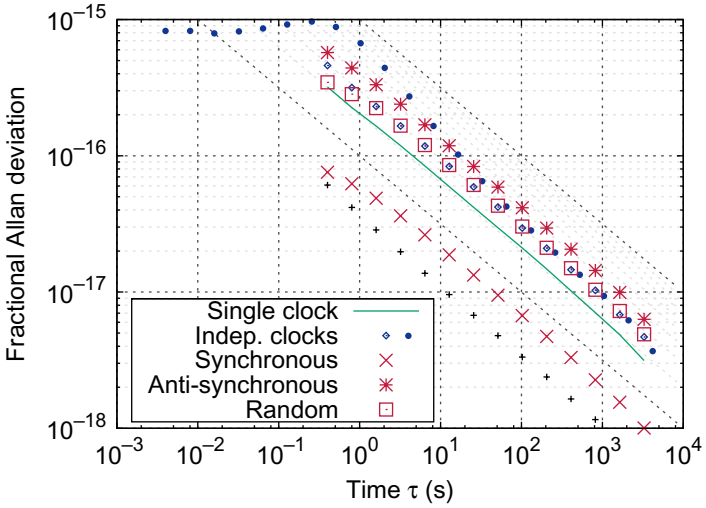

Figure 7. Comparison of two Sr lattice clocks with parameters $T_c = 400\,\text{ms}$, $d = 0.5$, $N = 10^4$ atoms and the same laser and detection noise as in figure 3 (left). The green line shows the asymptotic frequency stability of a single clock. Blue points show the asymptotic (output 1, ◇) and actual (output 2, •) frequency stabilities of the beat between two independent clocks. Red points show the frequency stability of the difference between the correction signals of two clocks operating with the same oscillator with three different sequence overlaps. The first points of these curves show the servo-loop bandwidth, whereas the subsequent behavior shows a $\tau^{-1/2}$ averaging. The black '+' shows the detection noise floor.

the difference signal is physically measurable even for short integration times τ, whereas the asymptotic behavior can only be determined in the limit where $\tau \gg T_c$.

Two independent clocks could also be used to simulate a dead-time free clock, by sampling the same oscillator over two complementary interrogation periods and by applying the summed correction of the two clocks (figure 6(c)). In this configuration, the effect of the laser frequency noise is completely suppressed in the asymptotic frequency stability, and the QPN limit could eventually be reached (figure 8). However, characterizing such a stability would require the availability of two pairs of identical clocks, making it difficult to realize experimentally.

8. Conclusion

In this paper, we reviewed several aspects of the stability of an optical lattice clock. An optimized clock sequence can take advantage of an ultra-stable laser and the non-destructive detection scheme we developed, to reach a stability as low as $10^{-16}\tau^{-1/2}$ as compared to a few $10^{-15}\tau^{-1/2}$ currently attained in ion clocks as well as current implementations of lattice clocks. In particular, the optimization of the clock cycle we performed spans over the possibility offered by the short clock cycle and the atom recycling properties of the non-destructive detection scheme. Finally, we described several comparison strategies for two optical lattice clocks that share the same clock laser. These strategies can effectively show the stability achieved by the clocks, as well as exhibit the QPN level in a synchronized operation.

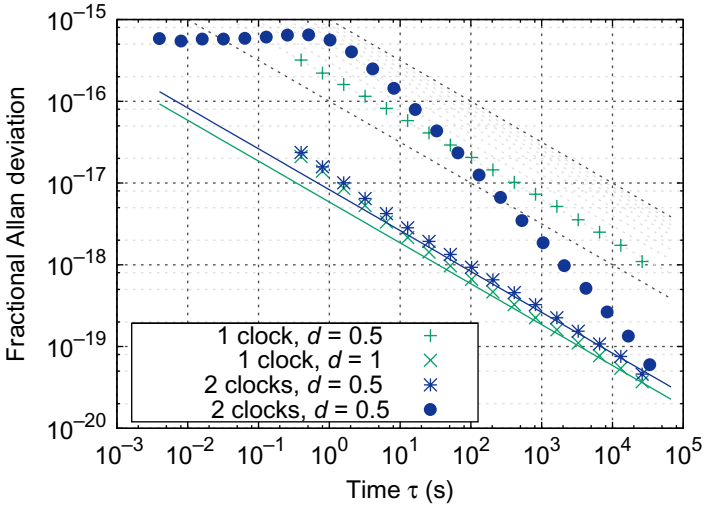

Figure 8. Laser stabilized by two lattice clocks with parameters $T_c = 400\,\text{ms}$, $N = 10^4$ atoms, a detection noise standard deviation of $25/N$ (purposely decreased from $200/N$ to exhibit the QPN floor; such a value can be envisioned with a non-destructive detection enhanced by a cavity) and a flicker noise level of $h_{-1} = 0.04\,\text{Hz}^2$ for the clock laser. The green points show the asymptotic frequency stability (output 1) for a single clock with a duty cycle of 0.5 (+) or 1 (×). The blue points show the the asymptotic stability (output 1, ∗) and the independently measured stability (output 2, •) for a single oscillator locked on two clocks with non-overlapping interrogation periods. The solid lines show the corresponding QPN levels. We can see from the asymptotic behavior that this scheme effectively simulates a dead-time free clock, except for a factor $\sqrt{2}$ that comes from the independently sampled QPN. The actual stability of the locked oscillator (•) shows that the QPN level at $3 \times 10^{-17}\tau^{-1/2}$ could be effectively reached after a few hours of integration time with an averaged stability of 10^{-19}.

Acknowledgments

SYRTE is a member of Institut Francilien de Recherche sur les Atomes Froids (IFRAF). This work was supported by funding from the European Community's Seventh Framework Programme, ERA-NET Plus, under Grant Agreement No. 217257, as well as from IFRAF, CNES and ESA.

References

[1] Marion H *et al* 2003 Search for variations of fundamental constants using atomic fountain clocks *Phys. Rev. Lett.* **90** 150801

[2] Santarelli G, Laurent Ph., Lemonde P, Clairon A, Mann A G, Chang S, Luiten A N and Salomon C 1999 Quantum projection noise in an atomic fountain: a high stability cesium frequency standard *Phys. Rev. Lett.* **82** 4619–22

[3] Wynands R and Weyers S 2005 Atomic fountain clocks *Metrologia* **42** S64–79

[4] Katori H, Takamoto M, Pal'chikov V G and Ovsiannikov V D 2003 Ultrastable optical clock with neutral atoms in an engineered light shift trap *Phys. Rev. Lett.* **91** 173005
[5] Hong F-L *et al* 2009 Measuring the frequency of a Sr optical lattice clock using a 120 km coherent optical transfer *Opt. Lett.* **34** 692–4
[6] Ludlow A D *et al* 2008 Sr lattice clock at 10^{-16} fractional uncertainty by remote optical evaluation with a Ca clock *Science* **319** 1805
[7] Baillard X *et al* 2008 An optical lattice clock with spin-polarized ^{87}Sr atoms *Eur. Phys. J. D* **48** 11
[8] Lemke N D, Ludlow A D, Barber Z W, Fortier T M, Diddams S A, Jiang Y, Jefferts S R, Heavner T P, Parker T E and Oates C W 2009 Spin-1/2 optical lattice clock *Phys. Rev. Lett.* **103** 063001
[9] Lisdat Ch., Vellore Winfred J S R, Middelmann T, Riehle F and Sterr U 2009 Collisional losses, decoherence and frequency shifts in optical lattice clocks with bosons *Phys. Rev. Lett.* **103** 090801
[10] Kohno T, Yasuda M, Hosaka K, Inaba H, Nakajima Y and Hong F-L 2009 One-dimensional optical lattice clock with a fermionic ^{171}Yb isotope *Appl. Phys. Exp.* **2** 072501
[11] Lemonde P and Wolf P 2005 Optical lattice clock with atoms confined in a shallow trap *Phys. Rev.* A **72** 033409
[12] Takamoto M, Hong F-L, Higashi R and Katori H 2005 An optical lattice clock *Nature* **435** 321–34
[13] Rosenband T *et al* 2008 Frequency ratio of Al^+ and Hg^+ single-ion optical clocks; metrology at the 17th decimal place *Science* **319** 1808–12
[14] Chou C W, Hume D B, Koelemeij J C J, Wineland D J and Rosenband T 2010 Frequency comparison of two high-accuracy Al^+ optical clocks *Phys. Rev. Lett.* **104** 070802
[15] Brusch A, Le Targat R, Baillard X, Fouché M and Lemonde P 2006 Hyperpolarizability effects in a Sr optical lattice clock *Phys. Rev. Lett.* **96** 103003
[16] Barber Z W, Stalnaker J E, Lemke N D, Poli N, Oates C W, Fortier T M, Diddams S A, Hollberg L, Hoyt C W, Taichenachev A V and Yudin V I 2008 Optical lattice induced light shifts in an Yb atomic clock *Phys. Rev. Lett.* **100** 103002
[17] Boyd M M, Zelevinsky T, Ludlow A D, Blatt S, Zanon-Willette T, Foreman S M and Ye J 2007 Nuclear spin effects in optical lattice clocks *Phys. Rev.* A **76** 022510
[18] Takamoto M, Hong F-L, Higashi R, Fujii Y, Imae M and Katori H 2006 Improved frequency measurement of a one-dimensional optical lattice clock with a spin-polarized fermionic ^{87}Sr isotope *J. Phys. Soc. Japan* **75** 104302
[19] Blatt S, Thomsen J W, Campbell G K, Ludlow A D, Swallows M D, Martin M J, Boyd M M and Ye J 2009 Rabi spectroscopy and excitation inhomogeneity in a one-dimensional optical lattice clock *Phys. Rev.* A **80** 052703
[20] Gibble K 2009 Decoherence and collisional frequency shifts of trapped bosons and fermions *Phys. Rev. Lett.* **103** 113202
[21] Rey A M, Gorshkov A V and Rubbo C 2009 Many-body treatment of the collisional frequency shift in fermionic atoms *Phys. Rev. Lett.* **103** 260402
[22] Yu Z and Pethick C J 2010 Clock shifts of optical transitions in ultracold atomic gases *Phys. Rev. Lett.* **104** 010801
[23] Petersen M, Chicireanu R, Dawkins S T, Magalhães D V, Mandache C, Le Coq Y, Clairon A and Bize S 2008 Doppler-free spectroscopy of the $^1S_0 - ^3P_0$ optical clock transition in laser-cooled fermionic isotopes of neutral mercury *Phys. Rev. Lett.* **101** 183004
[24] Dick G 1987 Local oscillator induced instabilities in trapped ion frequency standards *Proc. Precise Time and Time Interval Meeting, Redondo Beach (US Naval Observatory, Washington, DC, 1988)* pp 133–47
[25] Santarelli G, Audoin C, Makdissi A, Laurent P, Dick G J and Clairon A 1998 Frequency stability degradation of an oscillator slaved to aperiodically interrogated atomic resonator *IEEE Trans. Ultrason. Ferroelectr. Freq. Control* **45** 887–94
[26] Takano T, Fuyama M, Namiki R and Takahashi Y 2009 Spin squeezing of a cold atomic ensemble with the nuclear spin of one-half *Phys. Rev. Lett.* **102** 033601

[27] Appel J, Windpassinger P J, Oblak D, Hoff U B, Kjrgaard N and Polzik E S 2009 Mesoscopic atomic entanglement for precision measurements beyond the standard quantum limit *Proc. Natl Acad. Sci.* **106** 10960–5

[28] Windpassinger P J *et al* 2008 Nondestructive probing of Rabi oscillations on the cesium clock transition near the standard quantum limit *Phys. Rev. Lett.* **100** 103601

[29] Schleier-Smith M H, Leroux I D and Vuletić V 2010 States of an ensemble of two-level atoms with reduced quantum uncertainty *Phys. Rev. Lett.* **104(7)** 073604

[30] Louchet-Chauvet A, Appel J, Jelmer Renema J, Oblak D and Eugene Polzik S 2009 Entanglement-assisted atomic clock beyond the projection noise limit arXiv.org:0912.3895

[31] Allan D W 1966 Statistics of atomic frequency standards *Proc. IEEE* **54** 221–30

[32] Young B C, Cruz F C, Itano W M and Bergquist J C 1999 Visible lasers with subhertz linewidths *Phys. Rev. Lett.* **82** 3799–802

[33] Stoehr H, Mensing F, Helmcke J and Sterr U 2006 Diode laser with 1 Hz linewidth *Opt. Lett.* **31** 736–8

[34] Ludlow A D, Huang X, Notcutt M, Zanon-Willette T, Foreman S M, Boyd M M, Blatt S and Ye J 2007 Compact, thermal-noise-limited optical cavity for diode laser stabilization at 1×10^{-15} *Opt. Lett.* **32** 641–3

[35] Numata K, Kemery A and Camp J 2004 Thermal-noise limit in the frequency stabilization of lasers with rigid cavities *Phys. Rev. Lett.* **93** 250602

[36] Millo J, Magalhaes D V, Mandache C, Le Coq Y, English E M L, Westergaard P G, Lodewyck J, Bize S, Lemonde P and Santarelli G 2009 Ultrastable lasers based on vibration insensitive cavities *Phys. Rev.* A **79** 053829

[37] Ido T and Reid D T (ed) 2009 *Time and Frequency Metrology II (Proc. SPIE)* **7431** 74310A–74310A-14

[38] Dawkins S T, Chicireanu R, Petersen M, Millo J, Magalhães D V, Mandache C, Le Coq Y and Bize S 2010 An ultra-stable referenced interrogation system in the deep ultraviolet for a mercury optical lattice clock *Appl. Phys. B: Lasers Opt.* **99(1–2)** 41–6

[39] Audoin C, Santarelli G, Makdissi A and Clairon A 1998 Properties of an oscillator slaved to a periodically interrogated atomic resonator *IEEE Trans. Ultrason. Ferroelectr. Freq. Control* **45** 877–86

[40] Greenhall C A 1998 A derivation of the long-term degradation of a pulsed atomic frequency standard from a control-loop model *IEEE Trans. Ultrason. Ferroelectr. Freq. Control* **45** 895–8

[41] Lodewyck J, Westergaard P G and Lemonde P 2009 Nondestructive measurement of the transition probability in a Sr optical lattice clock *Phys. Rev.* A **79** 061401

[42] Westergaard P G, Lodewyck J and Lemonde P 2010 Minimizing the Dick effect in an optical lattice clock *IEEE Trans. Ultrason. Ferroelectr. Freq. Control* **57(3)** 623–8

[43] Martinez de Escobar Y N, Mickelson P G, Yan M, DeSalvo B J, Nagel S B and Killian T C 2009 Bose–Einstein condensation of ^{84}Sr *Phys. Rev. Lett.* **103** 200402

[44] Stellmer S, Tey M K, Huang B, Grimm R and Schreck F 2009 Bose–Einstein condensation of strontium *Phys. Rev. Lett.* **103** 200401

[45] Mukaiyama T, Katori H, Ido T, Li Y and Kuwata-Gonokami M 2003 Recoil-limited laser cooling of Sr^{87} atoms near the fermi temperature *Phys. Rev. Lett.* **90** 113002

[46] Brusch A, Targat R L, Baillard X, Fouché M and Lemonde P 2006 Hyperpolarizability effects in a Sr optical lattice clock *Phys. Rev. Lett.* **96** 103003